Annals of Biomedical Engineering
https://doi.org/10.1007/s10439-023-03348-1

BMES BIOMEDICAL ENGINEERING SOCIETY

ORIGINAL ARTICLE

Switching the Left and the Right Hearts: A Novel Bi-ventricle Mechanical Support Strategy with Spared Native Single-Ventricle

Emrah Şişli[1] · Canberk Yıldırım[2] · İbrahim Başar Aka[3] · Osman Nuri Tuncer[4] · Yüksel Atay[4] · Mustafa Özbaran[5] · Kerem Pekkan[6]

Received: 30 January 2023 / Accepted: 9 August 2023

Abstract

End-stage Fontan patients with single-ventricle (SV) circulation are often bridged-to-heart transplantation via mechanical circulatory support (MCS). Donor shortage and complexity of the SV physiology demand innovative MCS. In this paper, an out-of-the-box circulation concept, in which the left and right ventricles are switched with each other is introduced as a novel bi-ventricle MCS configuration for the "failing" Fontan patients. In the proposed configuration, the systemic circulation is maintained through a conventional mechanical ventricle assist device (VAD) while the venous circulation is delegated to the native SV. This approach spares the SV and puts it to a new use at the right-side providing the most-needed venous flow pulsatility to the failed Fontan circulation. To analyze its feasibility and performance, eight SV failure modes have been studied via an established multi-compartmental lumped parameter cardiovascular model (LPM). Here the LPM model is experimentally validated against the corresponding pulsatile mock-up flow loop measurements of a representative 15-year-old Fontan patient employing a clinically-approved VAD (Medtronic-HeartWare). The proposed surgical configuration maintained the healthy cardiac index (3–3.5 l/min/m^2) and the normal mean systemic arterial pressure levels. For a failed SV with low ejection fraction (EF = 26%), representing a typical systemic Fontan failure, the proposed configuration enabled a ~ 28 mmHg amplitude in the venous/pulmonary waveforms and a 2 mmHg decrease in the central venous pressure (CVP) together with acceptable mean pulmonary artery pressures (17.5 mmHg). The pulmonary vascular resistance (PVR)—SV failure case provided a ~ 5 mmHg drop in the CVP, with venous/pulmonary pulsatility reaching to ~ 22 mmHg. For the high PVR failure case with a healthy SV (EF = 44%) pulmonary hypertension is likely to occur as expected. While this condition is routinely encountered during the heart transplantation and managed through pulmonary vasodilators a need for precise functional assessment of the spared failed-ventricle is recommended if utilized in the PVR failure mode. Comprehensive *in vitro* and *in silico* results encourage this novel concept as a low-cost, more physiological alternative to the conventional bi-ventricle MCS pending animal experiments.

Keywords Single-ventricle physiology · Fontan circulation · Hemodynamics · Ventricle assist devices · Mechanical circulatory support · Mock-up flow loops · Lumped parameter modelling · Congenital heart surgery · Cardiovascular circulation theory

Abbreviations

BiVAD	Biventricular assist device
CA	Common atrium
CI	Cardiac index
CO	Cardiac output
CPB	Cardiopulmonary bypass
CVP	Central venous pressure
EF	Ejection fraction
HR	Heart rate
LPM	Lumped parameter model
LVAD	Left ventricle assist device
MCS	Mechanical circulatory support
PA	Pulmonary artery
PVR	Pulmonary vascular resistance
RV	Right ventricle
RVAD	Right ventricle assist device
SV	Single ventricle

Associate Editor Lakshmi Prasad Dasi oversaw the review of this article.

This study is conducted through joint corresponding authors Emrah Şişli and Kerem Pekkan.

Extended author information available on the last page of the article

Published online: 27 August 2023

SVR	Systemic vascular resistance
TCPC	Total cavopulmonary connection
VAD	Ventricle assist device

Introduction

Each year, about 8 in a 1000 babies are born with a clinically-significant congenital heart defect [5, 6, 17, 24, 25, 44]. The most serious structural heart defects require complex palliative surgical reconstructions with the aim to achieve an optimally working blood circulation with the only available single-ventricle (SV). These surgical reconstructions are performed in series to gradually compensate the missing right-heart. The final surgical stage is the Fontan procedure [14, 15] first performed in 1971. Following this pioneering surgical procedure, advances in pediatric cardiac surgery have resulted in reduced morbidity and mortality in this vulnerable patient group [3, 26, 27, 32–34]. Unfortunately, the current surgical therapy is palliative; as the child grows, due to vascular remodeling and hemodynamic adaptations, this complex and surgically reconstructed physiology gradually fails. Presenting severe complications related to the gastrointestinal system, including feeding disorders, liver dysfunction, protein losing enteropathy, and plastic bronchitis [43].

As almost all SV patients eventually require either heart transplantation or mechanical circulatory support (MCS) in their late adulthood [26], the steadily increasing number of "Fontan survivors" with poor quality-of-life is an emerging global health challenge [47, 49, 61], shortage of donor organ supply has made MCS an inevitable surgical tool for bridge-to-transplantation to improve a patient's transplant candidacy [1, 62]. While a variety of surgical concepts using pulsatile- or continuous flow MCS devices are being proposed [16, 25, 46, 63], novel approaches and breakthrough devices are particularly desired to address the physiology-related limitations of the declining SV circulation. For example, Giridharan et al. introduced a low blood damage pump without an impeller [18] and our research group proposed an implantable Fontan ventricle assist device (VAD) without the need for an external power, resembling a turbocharger [38]. Likewise, other novel devices employing the jet-pump principles is being refined for Fontan assist [41]. Cannulated TCPC support emerged as an alternative approach and custom cannulation designs and unique configurations are tested *in vitro* with limited failed-circulation cases [57]. For example, Professor Amon's research team considered a triple lumen cannula attached to an external right-heart centrifugal blood pump [31]. Wang et al. modified an Avalon DLP cannula and tested it in a piglet TCPC model [60].

Computational fluid dynamic analysis, provide rich information on local Fontan assist device hemodynamics, which is extremely useful for MCS design and optimization [19, 55]. As such, the system-level development of the emerging devices requires lumped parameter numerical modeling (LPM) delivering rapid results. The first SV LPM analysis study that demonstrated the VAD coupling to a Fontan pathway considered a hemodynamically functioning "optimized" Fontan circulation [39]. Exercise and the shape of the assist-device pressure–flowrate characteristics are studied next illustrating the need for precise coupling between the systemic and pulmonary flows realized through hemodynamic sensors [20]. SV-LPM modeling further applied to the first-stage surgical interventions [50] and expanded to incorporate failed/non-functional SV circulation states [8, 9]. For example, Durham et al. conducted a patient-specific LPM modeling campaign to test the HeartMate II pump at systemic support configuration against seven failed Fontan patients [11]. This study demonstrated the heterogeneous nature of Fontan failure modes influencing the VAD outcome. More recently, Farahmand et al. [13] recovered an ideal SV circulation from a moderately failed state using two subpulmonary support configurations of the Fontan pathway. Despite these investigations on failed-Fontan circulation with MCS support, a sequential SV disease transition model, starting from the pre-surgery state to final severe failed-Fontan did not exist in literature and the detailed clinical variations of the fundamental Fontan failure modes are not considered yet. These aspects will be investigated in the present paper.

In general, the major weakness of LPM modeling, as observed in literature, is the lack of *in vitro* validation. Apart from a single study where LPM results are compared with the physiological measurements obtained from an acute Fontan animal model with VAD [7], only a few *in vitro* mock-up studies with the actual VADs are tested in the Fontan (SV) circulation [10, 58]. Thus another aim of the present study is to expand our experience with LPM validation specifically focusing consequently failed Fontan states.

Although the failure of Fontan circulation is multifactorial; including conditions that affect pulmonary vascular bed and systemic pump (namely the myocardium, valves, and rhythm) [1, 6, 24, 32, 38, 47], the chronic long-standing privation of the pulsatile pulmonary blood flow in Fontan circulation is considered one of the main reasons of the Fontan failure [39, 40, 46, 47]. Achieving physiological pulsatility levels at the right side is paramount to preserve the healthy pulmonary, and lymphatic function of Fontan patients [47]. Apart from the Berlin Heart [21], external valved-compression devices [23, 28] and precisely timed cuffs [59, 64], the majority of clinically available MCS strategies result steady flow. To address the long-sought venous pulsatility, in this study, we introduce a novel Fontan-MCS modification that can provide the desired physiological "native

right ventricle-like" pulsatile flow to support and *gradually heal* the Fontan failure. Hemodynamic characteristics of this concept was analyzed focusing primarily on the early stage failed Fontan patients that display systemic heart failure (American Heart Association Class II/Class III [22]), in whom a left ventricular mechanical assist device is normally considered as a bridge-to-heart transplantation (Fig. 1a). The concept was also tested for the high-PVR Fontan failure model. We hypothesize that in combination with the conventional left VAD therapy, rather than discarding the native SV, sparing it for the right heart support would result the desired venous hemodynamics (Fig. 1b). Furthermore, in some patients, where a bi-ventricle MCS support is essential, this approach will provide significant cost savings that is much significant for resource-limited settings with limited access to MCS devices.

To the best of our knowledge, there is no available technique for failing Fontan patients in whom the systemic circulation is maintained by a standard MCS, and the cavopulmonary circulation is delegated to the native SV as illustrated in Fig. 1b. In this manuscript, analyses were performed for an optimal "baseline" Fontan circulation, clinically meaningful variations of high PVR and ventricular dysfunction (VD) Fontan failures. These new failure modes were also examined under the conventional support and the proposed modification, using the actual clinically approved device (HeartWare HVAD, Medtronic, US), both *in vitro* and *in silico*. An established experimental Fontan mock-up flow loop and a computational LPM originally developed for Fontan circulation were used to investigate a variety of clinically significant states.

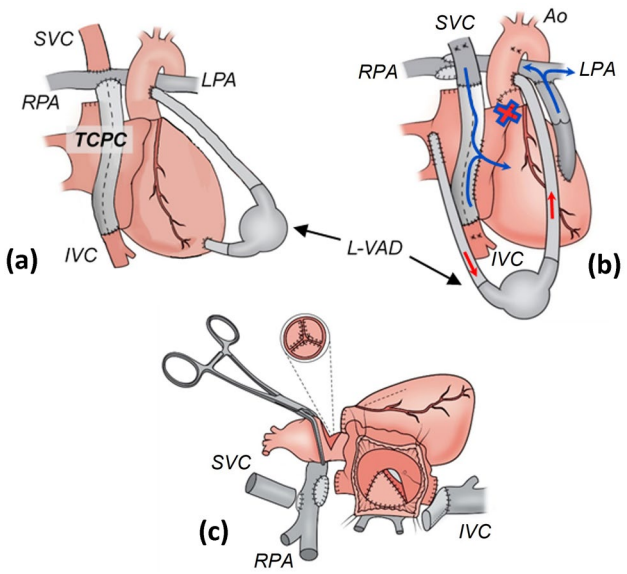

Fig. 1 **a** Traditional left ventricle assist device (LVAD) implantation configuration for systemic single-ventricle (SV) failure of the total cavopulmonary (TCPC) circulation. **b** Proposed configuration where the native SV is utilized as a pulsatile right heart. To achieve this, Fontan (TCPC) tube graft is anastomosed to the right atrium, systemic circulation is maintained by LVAD from pulmonary venous chamber to aorta (Ao), and pulmonary circulation is delegated to the SV via a conduit interposed between the SV and pulmonary artery bifurcation. Blood flow directions are labeled with arrows. **c** A sketch displaying the surgeons view is provided during the take-down of TCPC anastomoses, patch plasty of the pulmonary artery, creation of a posteriorly placed pulmonary venous chamber, and aortic valve closure through aortotomy (*LPA* left pulmonary artery, *RPA* right pulmonary artery, *IVC* inferior vena cava, *SVC* superior vena cava)

Methods

Surgical Technique

Through a traditional redo cardiac surgery approach, following aortic and selective bi-caval cannulation, cardiopulmonary bypass (CPB) is established. Under total CPB, the Fontan tube graft and superior cavopulmonary anastomosis are taken down from the right PA. The defects remained in the PA are patch repaired. The superior vena cava is anastomosed to the cephalic side of the Fontan tube graft. The aorta is cross clamped, and electromechanical quiescence is achieved by cardioplegia. Through right atriotomy, a patch is fashioned to fit for isolation of the pulmonary veins posterior to the left atrium. The aortic valve is closed through an aortotomy (Fig. 1c). The Fontan tube graft is anastomosed side-by-side to the right atrium. Following a systemic ventriculotomy performed at the base of the heart, an appropriately-sized valved-conduit is interposed between the SV and the PA bifurcation. After priming of the MCS device, the outflow graft is anastomosed to the ascending aorta, and the inflow graft anastomosis to the left atrium is completed. Following removal of the aortic cross-clamp, the CPB flow is gradually reduced while the flow of the MCS device is increased synchronously (Fig. 1c). By this way, left (via MCS device) and right sides (via SV) are totally separated like a biventricular circulation, providing a Q_p/Q_s ratio of 1.

Lumped Parameter Fontan Circulation Model

An established multi-compartmental LPM developed by our group for congenital heart disease research [65, 66] has been adopted to simulate the proposed surgical configuration and Fontan circulation states. This model computes the pressure and flow waveforms for key vascular components by representing them as compliance chambers and resistance vessels as given in Eq. (1).

$$\frac{\mathrm{d}(CP)_i}{\mathrm{d}t} = \sum_{j=1}^{N} \frac{P_j - P_i}{R_{ji}} + Q_{\mathrm{pump,ji}}, \tag{1}$$

where C and P are the compliance and pressure of the compliant chamber represented by the index (i or j), respectively. R is the peripheral resistance of the vessel connecting the associated chambers. N is the number of lumped elements. Q_{pump} is the flow of the MCS device and dt is simulation time step. Pump speed was determined based on the required Q_{pump} as explained in the following section and remained constant during the analysis. Backward Euler method was used to iteratively solve the implicit formulation of Eq. (1) using the fixed time step.

Compliance of the chambers are set as constant values based on the baseline patient profile (Table 1 and Supplementary File 1 attached to the Data availability section). SV model function is modeled through the time-varying elastance concept introduced by Suga et al. [54] [$E_{\mathrm{SV}}(t)$] and the "double-Hill" function $E_n(t_n)$ described by Stergiopulos et al. [53] as in Eq. (2). Double-Hill function resolved ventricle characteristics reasonably well as presented in our earlier articles [37, 65, 66].

$$E_{\mathrm{SV}}(t) = \left(E_{\max} - E_{\min}\right)E_n(t_n) + E_{\min}. \tag{2}$$

All the simulations and measurements were based on a 15-year-old (1.44 m^2) Fontan patient (Table 1), the age of which was considered as an approximate age of Fontan failure [12, 38]. Cardiac functions, SVR and PVR were tuned according to the body size of the chosen patient profile.

Mechanical Circulatory Support Characteristic Module

For all LPM cases, the pump model employs a quadratic pressure drop–flow rate relation, which was derived based on our previous work [39], as follows:

$$\begin{aligned}\Delta P_{ji} = {} & \rho w^2\left(r_{\mathrm{out}}^2 - r_{\mathrm{in}}^2\right) - Q_{\mathrm{pump,ji}} \\ & \left(\frac{\rho w r_{\mathrm{out}}}{2\pi r_{\mathrm{out}} b_{\mathrm{out}} \tan(\beta_{\mathrm{out}})} - \frac{\rho w r_{\mathrm{in}}}{2\pi r_{\mathrm{in}} b_{\mathrm{in}} \tan(\beta_{\mathrm{in}})}\right) \\ & - {Q_{\mathrm{pump,ji}}}^2\left(\rho f \frac{L}{2DA^2}\right),\end{aligned} \tag{3}$$

where w is the rotational speed, r is the pump impeller radius, b is the blade width and β is the blade angle. In surface friction term, f is the pump friction factor, L is the approximate blade length, D is the hydraulic diameter and A is the flow area. out index represents the value at pump outlet while in index represents the associated parameter at the inlet.

When the order of magnitudes are considered, second term of the Eq. (3) is negligible. Therefore, using the available approximate values of these parameters specifically for HVAD HeartWare ($r_{\mathrm{out}} = 15.5\mathrm{mm}$, $r_{\mathrm{in}} = 9\mathrm{mm}$, $\beta_{\mathrm{out}} = 45^{\circ}$, $\beta_{\mathrm{in}} = 60^{\circ}$, $b_{\mathrm{out}} = b_{\mathrm{in}} = 5\mathrm{mm}$, $f = 0.035$, $D = 8.3\mathrm{mm}$, $L = 263\mathrm{mm}$, $A = 54.1\mathrm{mm}^2$), *in silico* pump characteristic curves were generated and compared with literature for selected rotational speeds, as shown in Fig. 2. It must be noted that, for the HeartWare—HVAD, the exact form of the neglected second term of Eq. (3) cannot be represented in an explicit mathematical form due to its unique impeller design. Still this neglected term is very small and do not influence the pump characteristic curves employed in this study.

Table 1 Cardiovascular anthropometric data of the idealized Fontan patient used in this study

Variable	Data
Age (years)	15
Height (cm)	150
Body weight (kg)	50
Body surface area (m^2)	1.44
Heart rate (bpm)	70
Cardiac index (l/min/m^2)	3
Common atrial volume (ml)	70
Systemic venous chamber volume (ml*)	45
Pulmonary venous chamber volume (ml*)	25

Parameters are compiled from literature and verified through clinical experience [1, 62]

*Corresponds to the venous chamber volumes after partitioning of the common atrium (CA) employed in cases *VD-switch*, *PVR-switch*, *bPVRtc-switch* and *bPVRtc-Pswitch*

Fontan Circulation States

Ideal Fontan Circulation (*Fontan*)

The compliance and resistance parameters of ideal Fontan circulation state, referred as *Fontan* throughout the manuscript, was modelled based on the Egbe et al. [12] and our previous LPM study [38]. 62 ml stroke volume and 44% ejection fraction (EF) was supplied by the SV. Cardiac parameters, systemic and pulmonary vascular resistances (SVR and PVR, respectively) were specified based on this representative patient (Table 1).

For this *baseline* case, the cardiac index (CI) was set to 3.0 l/min/m^2, and the systolic, diastolic, and mean aortic pressures were set to 100 mmHg, 67 mmHg, and 82 mmHg, respectively, which includes the exercise reserve. The corresponding LPM network and the *in vitro* mock-up flow loop

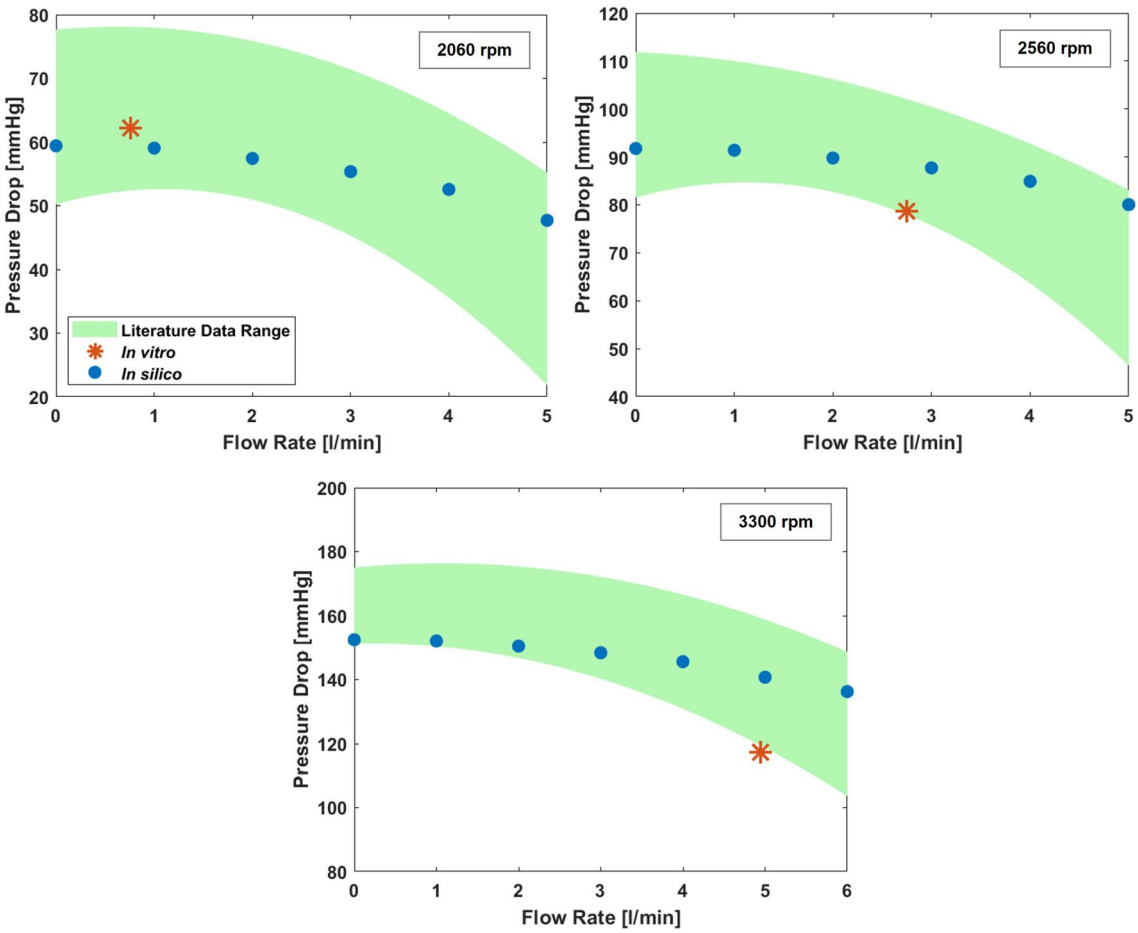

Fig. 2 *In silico* HeartWare HVAD characteristic curves and *in vitro* measurements with the literature data range [2, 27, 33, 35, 45] for w = 2060 rpm, 2560 rpm (used in case *VD-cmcs*) and w = 3300 rpm (used in case *VD-switch*). Red Asterix represents our measurements from the pump used during in vitro experiments

constructed for this baseline Fontan circulation is provided in Figs. 3a and 4a, respectively.

Fontan Failure, Ventricular Dysfunction (VD)

This circulation case was generated based on a moderate-to-severe VD (Class II/Class III) as classified by the American Heart Association [22]. Case *VD* was analyzed as two new *VD-Ac* and *VD-Cr* cases considering both the acute and chronic effects of the ventricular failure, respectively.

In *VD-Ac*, stroke volume used in *Fontan* case was reduced from 62 to 38 ml by decreasing the SV compliance, which leads to an EF of 26%. Therefore, acute effect of the ventricular failure was simulated. In *VD-Cr*, besides decreasing the EF, physiologic response of cardiovascular system to the acute decrease in aortic pressure and CI was studied. Such drop was compensated by increasing SVR index from 22.8 to 27.6 WU/m^2. Rest of the compliance and resistance parameters are kept as same with the *Fontan* case.

Following *VD* cases introduced in this study (*VD-cmcs* and *VD-switch*) were built on *VD-Cr* case, therefore, compliances and resistances were remained constant in these cases.

Fontan Failure, Increased Pulmonary Vascular Resistance (PVR)

In *PVR* case, another common mode of Fontan failure was established through high PVR index based on Egbe et al. [12]. It was analyzed through cases *PVR-Ac* and *PVR-Cr* considering the acute and chronic effects of the high PVR index, respectively.

In *PVR-Ac*, PVR value in *Fontan* case was increased from 1.65 to 3.3 WU/m^2 to simulate the acute (sudden) effect of the PVR related Fontan failure. Whereas in *PVR-Cr*, as observed in Fontan patients, SVR index and systemic venous compliance were both increased by approximately 10% besides doubling the PVR to replicate the physiological cardiovascular system response to preserve the cardiac output (CO) and

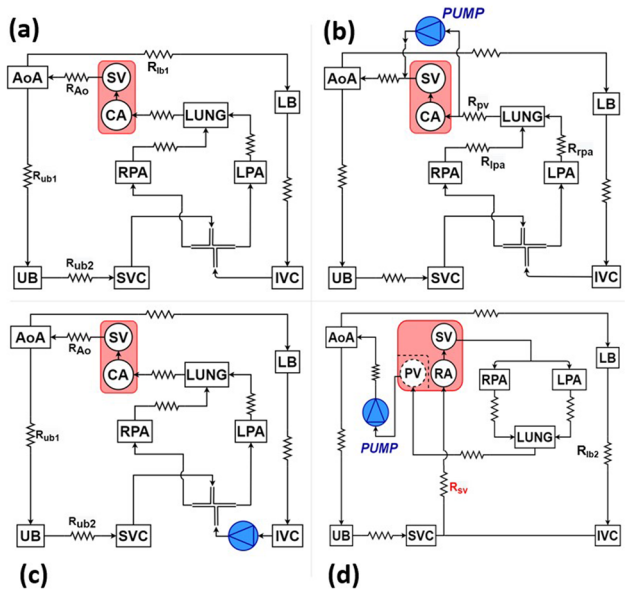

Fig. 3 Electrical analog circulation networks analyzed in this study. **a** Healthy and failed Fontan circulations (Cases: *Fontan*, *VD* and *PVR*), **b** conventional mechanical circulatory support (MCS) of ventricular dysfunction Fontan failure, Case: *VD-cmcs*. **c** Conventional MCS of increased PVR Fontan failure, Case: *PVR-cmcs* and **d** the proposed MCS modification cases *VD-switch* and *PVR-switch*. *SV* single ventricle, *CA* common atrium, *AoA* aortic arch, *LB* (*UB*) lower (upper) body, *IVC* (*SVC*) inferior (superior) vena cava, *RPA* (*LPA*) right (left) pulmonary artery, *LUNG* lungs, *PV* posterior pulmonary venous (surgically separated from the CA with the dashed lines), *RA* right atrium, R_{Ao} aorta resistance, R_{lb} (R_{ub}) lower (upper) body resistances, R_{TCPC} TCPC resistance, R_{rpa} (R_{lpa}) right (left) pulmonary artery resistance, R_{sv} systemic venous resistance, R_{pv} pulmonary venous resistance

systemic arterial pressure. Rest of the compliance and resistance parameters are kept as same with the *Fontan* case.

Following *PVR* cases introduced in this study (*PVR-cmcs* and *PVR-switch*) were built on *PVR-Cr* case, therefore, compliances and resistances were remained constant in these cases.

Conventional Mechanical Circulatory Support of the Ventricular Dysfunction Fontan Failure (*VD-cmcs*)

Case *VD-cmcs* corresponds to the conventional MCS (cmcs) of the Fontan failure state introduced in *VD-Cr*. In this configuration, MCS device supports the systemic circulation by working in parallel to the failing SV (EF = 26%), as shown in Figs. 3b and 4b. The device was operated at 2560 rpm, which provided a flow rate of 2.82 l/min to support the VD in terms of pressure and flow rate needs.

Conventional Mechanical Circulatory Support of the Fontan Failure with Increased Pulmonary Vascular Resistance (*PVR-cmcs*)

The conventional MCS support strategy intended for the high PVR Fontan failure model as introduced in *PVR-Cr* is simulated. Using our earlier cavopulmonary Fontan support framework [39, 66], MCS device was integrated between the systemic venous and pulmonary artery (PA), as shown in Fig. 3c.

In *PVR-cmcs*, both continuous and pulsatile flow MCS device operation was investigated. For continuous flow support, MCS device was operated at a constant rotational speed of 1205 rpm. To impose the pulsatile operation condition, the rotational speed of MCS device was modulated sinusoidally (±400 rpm) during the operation. MCS device provided a flow rate of 3.0 l/min to decrease the central venous pressure (CVP) and support the cavopulmonary circulation in both operation conditions.

Proposed Modification, Tested for Ventricular Dysfunction Failure (*VD-switch*)

Case *VD-switch* represents the application of proposed modification to the Fontan failure mode introduced above as *VD-Cr*.

Here, a 25 ml volume was isolated surgically from the total common atrium (CA) volume (70 ml) to form a neo-pulmonary venous return chamber. The remaining portion of CA serves as a right atrium. Systemic venous return was redirected to the new right atrium, after detaching it from the conventional total cavopulmonary connection (TCPC). Thus, systemic and pulmonary circulations become parallel similar to a normal biventricular circulation. SV was connected to PA to maintain the pulmonary circulation. Systemic circulation was governed by the MCS device having an inlet draining from the neo-pulmonary venous chamber, yet its outlet was placed to the aorta, functioning like a native left ventricle. MCS device was set to work at 3300 rpm, which provided a total CO of 4.95 l/min to the systemic circulation. In Fig. 1b, a cartoon representation of the proposed modification is provided together with surgical details in Fig. 1c. The corresponding circuit analogue is provided in Fig. 3d as used in LPM computations.

Performance of the modification in case *VD-switch* was also investigated during the metabolic activity. To perform a simple leg activity (walking function), the exercise protocol introduced by Kung et al. [29] for Fontan patients was used. Based on this protocol, from rest (MET = 0.65) to mild lower

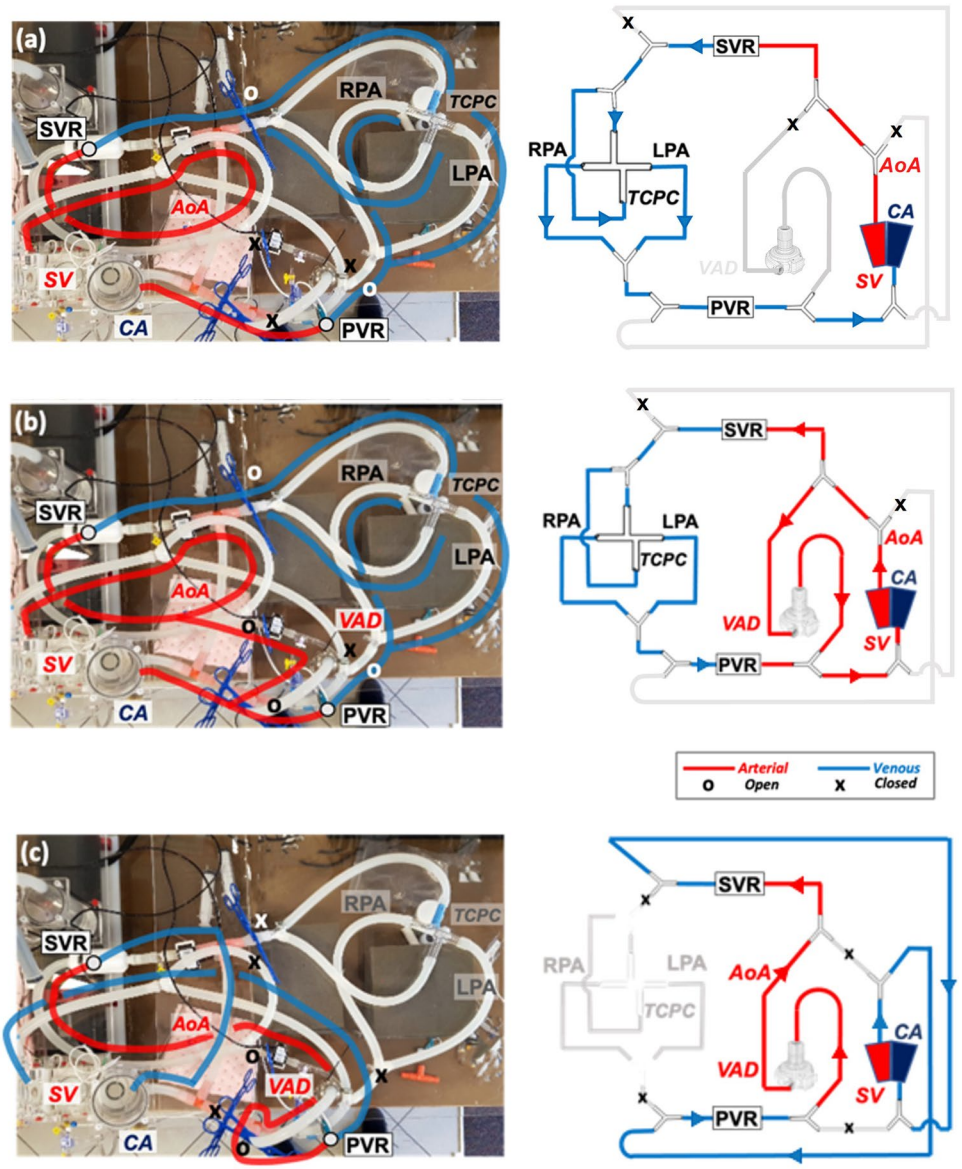

Fig. 4 Fontan circulation cases replicated experimentally in our mock-up flow loop for *in vitro* validation experiments. In a typical experimental run, cases are simulated in-sequence to allow direct comparison of measurements with each other. Starting with the **a** ideal, baseline *Fontan* circulation followed by the ventricular dysfunction failure case: *VD*, **b** MCS of ventricular dysfunction failure (*VD-cmcs*) and **c** the current modification where the MCS device operates as the left ventricle and the single-ventricle (SV) operates as the right ventricle (Case: *VD-switch*). *Red* and *blue lines* indicate the systemic and pulmonary circulations, respectively. *Gray colored lines* for the baseline Fontan network were removed in *VD-switch* configuration. *SVR* systemic vascular resistance, *PVR* pulmonary vascular resistance, *RPA* right pulmonary artery, *LPA* left pulmonary artery, *Ao* aorta, *TCPC* total cavopulmonary connection, *CA* common atrium, *VAD* ventricle assist device (HeartWare HVAD from Medtronic)

body exercise (MET = 5), all parameters were remained constant except that the HR was increased from 66 to 130 bpm and SVR was decreased by 15%.

Proposed Modification, Tested for the Increased Pulmonary Vascular Resistance (*PVR-switch*)

Here the proposed modification was applied to the high PVRI failure Fontan model introduced in *PVR-Cr*. MCS device governing the systemic circulation was operated at 3175 rpm corresponding to the flow rate of 4.32 l/min.

PVR-switch was also investigated for the activated compensatory mechanisms through *bPVRtc-switch*. In this case, heart rate (HR) was increased from 70 to 120 bpm. Moreover, PA banding was applied to avoid an excessive increase in pulmonary pressure. Analysis in *bPVRtc-switch* was repeated with the pulsatile MCS device operation introduced in *bPVRtc-Pswitch*. To observe the effect of pulsatility on the aortic flow and pressure, rotational speed of the device was modulated sinusoidally (±400 rpm) during the course of operation.

All cases are summarized in Table 2.

In Vitro Mock-Up Circuit

Computational simulations are tested against the mock-up experimental measurements. For this validation campaign, the pediatric pulsatile mock-up flow loop was operated under the same VD and MCS conditions of the LPM model for the ideal/functional (*Fontan*), *VD*, conventionally assisted VD (*VD-cmcs*) and the proposed modification assisted VD (*VD-switch*) cases. This bench-top circulation system included a compliant ventricular phantom and computer-controlled pulse-duplicator (SuperDup'r, Vivitro Systems, Inc., BC, Canada), which set the pulsatile flow rate by adjusting stroke and stroke volume, as described in our previous publications [10, 38]. As per our experimental protocol, Fontan circuits were generated in sequence using clamps and Y-branches without significantly altering the circuit parameters or stopping the piston-pump, as seen in Fig. 4. Thus, all the tested cases were comparable with each other and corresponded to the early acute changes of the proposed configuration. *In vitro* compartmental resistance and compliance values were same as in our previous mock-up Fontan circulation study [38] kept constants for all cases. These compartment parameters were adjusted representing the combination of lumped chambers in Fig. 3 for sake of simplicity, so that these lumped chambers are not separately represented in Fig. 4. Experiments are conducted using clamps so that different cases can be realized without stopping the pulsatile pump and keeping the same circulation parameters.

Our previously used standard 13.3 mm diameter 1° offset based on the chest MRI of a Fontan patient TCPC connection made of glass was attached to inferior/superior vena cava and right/left PA compliance chambers [40]. Two clamp-on ultrasonic pulsatile flow transducers, namely a 3PXL to the pump outlet and an 8PXL to the aorta were then connected to TS410 flow modules (Transonic Systems, Inc., Ithaca, New York), which were placed downstream of the SVR and MCS device outlets. Pressure measurements (Deltran 6200, Utah Medical Products, Inc., Midvale, Utah) were obtained from the SV, aorta, MCS device outlet, pulmonary venous chamber and systemic venous bed. CVP was obtained from the pressure sensor placed on the inferior vena cava part of the Y-branch right after SVR. Measurements were recorded using the LabChart Data Acquisition Unit (AD Instruments, Colorado Springs, Colorado). Distilled water was used in the *in vitro* experiments at room temperature.

To investigate the proposed modification in a comparative manner, the same MCS device, HeartWare HVAD (Medtronic, Inc., Fridley, Minnesota), was used for all *in silico* and *in vitro* cases. Therefore, pressure and flow hemodynamics are the main metrics to evaluate the performance of the modification subject to different circulation parameters or common disease states.

Table 2 The clinically significant Fontan circulation states that are analyzed in this study are summarized

Fontan	Ideal (optimally functioning) Fontan circulation. Corresponds to a time-point long after the third stage surgery. That is, immediate effects of establishing full single-ventricle (SV) circulation after surgery is recovered (e.g. low post-op. cardiac output)
VD	
VD-Ac	*Fontan Failure Mode 1* SV systemic dysfunction associated failure of the Fontan circulation. Acute state is simulated, suddenly after the initiation of failure
VD-Cr	*Fontan Failure Mode 1* SV systemic dysfunction associated failure of Fontan circulation. Chronic state is simulated, long-term after the failure
PVR	
PVR-Ac	*Fontan Failure Mode 2* high PVR associated failure of Fontan circulation. Acute state is simulated, suddenly after the initiation of failure
PVR-Cr	*Fontan Failure Mode 2* high PVR associated failure of Fontan circulation. Chronic state is simulated, long-term after the failure
VD-cmcs	Conventional systemic support strategy for Fontan Failure Mode 1 (*VD-Cr*). Includes a clinical ventricle assist device (VAD) supporting systemic circulation
PVR-cmcs	Conventional TCPC support strategy for Fontan Failure Mode 2 (*PVR-Cr*). Includes a Fontan assist device (FVAD) at the right-side, replacing TCPC conduit
VD-switch	Proposed Fontan support strategy employing the native SV for Fontan Failure Mode 1 (*VD-Cr*). Hemodynamic performance is compared with Case *VD-cmcs*
PVR-switch	Proposed Fontan support strategy employing the native SV for Fontan Failure Mode 2 (*PVR-Cr*). Hemodynamic performance is compared with Case *PVR-cmcs*
bPVRtc-switch	Proposed support strategy for Fontan failure in (*PVR-Cr*) but with PA banding and tachycardia
bPVRtc-Pswitch	Repetition of (*bPVRtc-switch*) with a pulsatile MCS device operation. Pulsatility is generated with sinusoidal rotational speed regulation

The case number names that are used throughout the text are provided in Column 1

Results

In Vitro Validation of Lumped Parameter Circulation Model

Ideal and VD Fontan failure models (*Fontan*, *VD*, *VD-cmcs* and *VD-switch*) were replicated exactly in an experimental mock-up circulation flow loop for numerical validation. For all cases, measured aortic pressure waveforms demonstrated acceptable agreement with *in silico* LPMs computations, as shown in Fig. 5. There is a small phase differences observed between the waveforms, which is based on the HR difference of 4% between *in silico* and *in vitro* simulations.

Likewise, simulated hemodynamics were also validated through pulsatile *in vitro* measurements. For the SV pressure, simulated and measured values in *Fontan* and *VD-switch* matched almost exactly. On the other hand, almost 6% difference between *in silico* and *in vitro* measurements is achieved both in *VD* and *VD-cmcs*. In terms of CVP, *in silico* results agreed well with *in vitro* measurements for *VD* and *VD-switch*. However, CVP revealed a difference of 11% and 17% between the *in silico* and *in vitro* for *Fontan* and *VD-cmcs*, respectively. In *VD-switch*, MCS device pressure was recorded to be 101 mmHg in both *in silico* and *in vitro* analyses, yet it revealed a difference of 3% in CI values. In *VD-cmcs*, the CI of 3.43 l/min/m^2 was observed in both *in silico* and *in vitro* simulations. This discrepancy (max. 6.5% observed between *in silico* and *in vitro*) is due to the MCS device pressure adjusted to provide the same CI. There was no significant difference (<1 mmHg) in pulmonary venous pressures between the *in vitro* and *in silico* models in all cases.

In all cases, a continuous flow MCS device, HeartWare HVAD (Medtronic) was used. However, a pulsatile aortic pressure waveform was observed through *in vitro* analysis in *VD-switch*, as seen in Fig. 5d. In this case, the pressure sensor placed at MCS device output in *in vitro* experiments was affected by the pulsating piston ventricle of the mock-up loop (Fig. 4c), which is the reason of such pulsatile aortic waveform. Therefore, even though the same mean aortic pressure was achieved, different waveforms was observed in *in silico* and *in vitro* results.

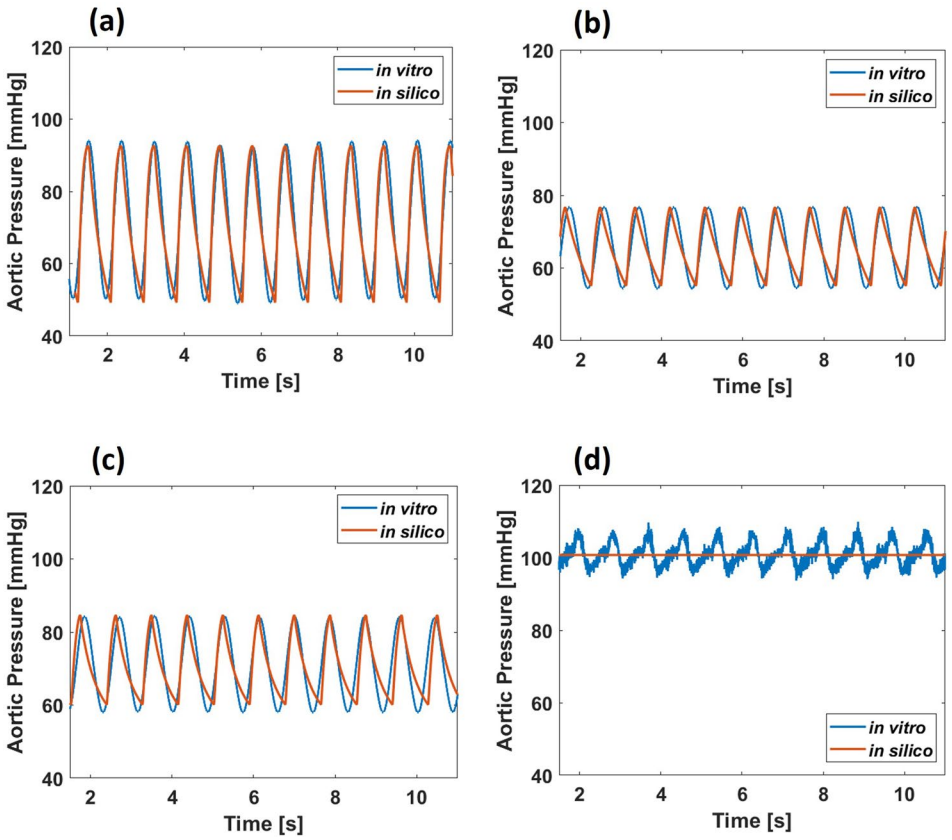

Fig. 5 Representative pressure waveforms obtained from the *in vitro* mock-up flow loop measurements and *in silico* LPM model computations are plotted for the circulation cases of **a** the healthy *baseline* (for ventricular dysfunction cases); *Fontan*, **b** ventricular dysfunction; *VD*, **c** conventional mechanical circulatory support of VD; *VD-cmcs* and **d** when the right-ventricle is used a right-heart in *VD* as proposed in this manuscript; *VD-switch*. All waveforms presented are recorded after the mock-up flow loop is stabilized and operating at the steady pulsatile hemodynamics

It is worth noting that the pressure drop based on the inertance of the tubes representing the cardiovascular elements in our *in vitro* setup was also estimated. The maximum inertance was observed at the tube representing the aorta, as expected, which has a length of 0.03 m and a radius of 0.007 m. The inertance of this section results a maximum pressure drop of only 4% of the mean aortic pressure. Likewise, the inertance based on pressure drop in the venous tubing components are observed to be 10^{-3} mmHg, primarily due to the low pulsatility. According to these observations, *in silico* and *in vitro* results were compared and agreed even though neglecting the inertance effect for simplicity.

Fontan Failure-1, Ventricular Dysfunction Model

Results associated with VD models (*VD*, *VD-cmcs* and *VD-switch)* are shown in Table 3.

In *VD*, EF of 26% led to a decrease in CI and aortic pressure by 1.7 l/min/m^2 and 5 mmHg, respectively. Since pumping energy (stroke volume) of the SV was reduced to decrease EF, CVP also decreased by 4 mmHg. Correspondingly, PA pressure decreased slightly from 11 to 9 mmHg.

In *VD-cmcs*, CI was increased by 1.7 l/min/m^2 with the conventional systemic support of MCS device. It augmented both the aortic and ventricular pressures by 5 mmHg and 4 mmHg, respectively. CVP pressure was barely increased due to the implantation configuration of MCS device in this case (Fig. 4b), unlike the conventional cavopulmonary support.

In *VD-switch*, MCS device directly reflects the pulmonary flow to systemic circulation. In pulmonary side, although the stroke volume of SV was nearly doubled, EF of it remained constant. Mean SV pressure was simulated as 18.5 mmHg. Additionally, PA pressure increased from 10.7 to 17.5 mmHg (39%). CVP was decreased by 2 mmHg (13%). *In silico* waveforms simulated for the VD model are shown in Fig. 6. As expected, suction effect of MCS device caused a decrease in pulmonary venous pressure to − 1.2 mmHg, almost collapsing the *in vitro* compliance chamber as seen in Fig. 6a. Nevertheless, CI and aortic pressure increased by 1.7 l/min/m^2 (doubled) and 25 mmHg (38%), respectively, to compensate for the low EF.

Fontan Failure-2, Increased Pulmonary Vascular Resistance Model

Hemodynamics associated with the high PVR index Fontan failure cases (*PVR-Ac/Cr*, *PVR-cmcs*, *PVR-switch*, *bPVRtc-switch* and *bPVRtc-Pswitch*) are presented in Table 4.

In *PVR-Ac*, a decrease in CI by 0.35 l/min/m^2 and mean aortic pressure by 7 mmHg was observed. CVP increased from 14 to 16.25 mmHg at this acute stage of failure. Elevated CVP also increased the PA pressure by 3 mmHg. In *PVR-Cr* representing the chronic condition, hemodynamic mechanisms tended to pull the systemic parameters to the ideal Fontan circulation by increasing the SVR index. Thus, CVP elevated from 14 to 18 mmHg, which led to the serious failure of Fontan circulation in time.

Table 3 Simulated hemodynamic parameters of the ventricular dysfunction Fontan failure state managed through conventional systemic support vs. the spared single-ventricle (SV) configuration

	(*VD-Cr*) ventricular dysfunction Fontan failure (chronic)	(*VD-cmcs*) conventional systemic MCS	(*VD-switch*) w/ spared SV proposed modification
HR (bpm)	66	66	66
EF (%)	26	26	26
Stroke volume index (ml/m^2)	26	22	43
CO (l/min)	2.47	4.93*	4.95
CI (l/min/m^2)	1.72	3.42	3.44
MCS device output (l/min)	n/a	2.82	4.95
SBP (mmHg)	77	85	101
DBP (mmHg)	55	60	101
MBP (mmHg)	65.5	71	101
CVP (mmHg)	10.8	11.35	12
PAP (mmHg)	9	7.85	17.5

Note that the ideal Fontan circulation hemodynamic parameters to impose ventricular dysfunction are nearly 10% higher than the used one for increased PVR model. Thus, this condition is not additionally given in this table. Figure 4a represents the waveform obtained for this *baseline* condition

CI cardiac index, *CMRI* cardiac magnetic resonance imaging, *CO* cardiac output, *CVP* central venous pressure, *DBP* diastolic blood pressure, *EF* ejection fraction, *HR* heart rate, *PAP* pulmonary artery pressure, *SBP* systolic blood pressure, *MBP* mean blood pressure, *MCS* mechanical circulatory support

*CO represents the total blood flow provided by the MCS device and SV

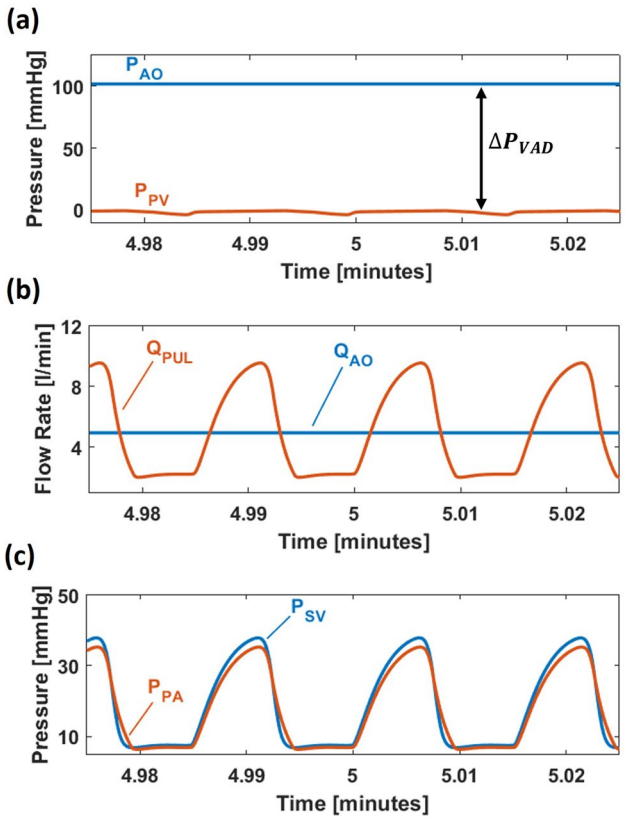

Fig. 6 Fontan Failure Mode 1. Representative hemodynamic waveforms when the ventricular dysfunction Fontan failure mode is bridged-to-transplant via the proposed spared single-ventricle (SV) MCS configuration. **a** Aortic (P_{AO}) and pulmonary venous (P_{PV}) chamber pressures, **b** aortic (Q_{AO}) and pulmonary (Q_{PUL}) flow waveforms with the MCS, **c** single ventricular (P_{SV}) and pulmonary artery (P_{PA}) pressure waveforms

In *PVR-cmcs*, CVP decreased by 3 mmHg (16.7%) with the cavopulmonary conventional MCS. Therefore, CI increased by 0.35 l/min/m^2 (12.5%) and the mean aortic pressure increased by 6 mmHg (7.3%). Using the MCS device as a right ventricle (RV) in this case also increased the PA pressure from 13.5 to 15 mmHg (11.1%).

In *PVR-switch*, the mean aortic pressure was observed as 78 mmHg with the CI of 3.0 l/min/m^2. The EF of the SV, which governs the pulmonary circulation remained as 43% while the MCSD propelled 4.32 l/min of blood to the systemic circulation. As a result, the desired systemic hemodynamic measurements as per aortic pressure and CI were obtained, which led to a decrease in CVP to 8.7 mmHg (38%). However, the PA pressure was excessively elevated to 42 mmHg as expected. First, nitric oxide vasodilation effect was imposed in our simulations through halving the PVR, however, this application was only able to reduce the PA pressure to 40 mmHg. Therefore, in *bPVRtc-switch*, such pulmonary hypertension was aimed to ease more significantly through tachycardia and PA banding, which led to a decrease in EF from 43 to 27%. Correspondingly, the PA pressure decreased to 37 mmHg from 42 mmHg, while the aortic pressure and CI remained nearly constant as in *PVR-switch*. Additionally, the CVP slightly increased to 9.1 mmHg.

In *bPVRtc-Pswitch*, an approximately ± 3 mmHg of pulsatility was generated in the pulmonary flow through replacement of the continuous flow MCS device with a pulsatile one. Since aortic compliance is less than the PA, only a pulsatility amplitude of 2 mmHg was observed in aortic pressure. The pulsatility in pulmonary flow was observed as ± 1.15 l/min. Although the application of a pulsatile MCS device did not significantly affect the mean aortic and PA pressures, it provided a more physiological systemic flow waveform. Figure 7 shows the effect of pulsatile MCS device on the hemodynamic waveforms in *bPVRtc-Pswitch*. Figure 7a represents the aortic and pulmonary venous pressure waveforms under the pulsatile pump effect. Assisted aortic and pulmonary flow waveforms are shown in Fig. 7b. Figure 7c demonstrated that the pulsatility generated by MCS device varied the blood flow rather than the compliance chamber pressure. Pulsatility of the PA pressure was approximately ± 9 mmHg. However, tachycardia and PA banding nearly eliminated the reverberation of it as seen in Fig. 7d.

Discussion

Use of a right-sided continuous flow MCS device supports reduces the venous pressure levels in Fontan failure, yet it lacks a physiological pulmonary flow. On the other hand, the proposed concept provides pulsatile pulmonary antegrade flow at physiological levels, which would also decrease pulmonary capillary recruitment and pulmonary vascular impedance [42, 54], eliminating the detrimental effects of non-pulsatile pulmonary flow [48]. This would potentially improve the condition of the patient gradually during bridge-to-heart transplantation.

Ventricular Dysfunction Failure Mode

Figure 6b, c demonstrated that the proposed use of spared SV in the VD Fontan failure (*VD-switch*) provided physiological PA pressure and pulmonary flow waveforms.

Table 4 Simulated hemodynamic parameters for high PVR Fontan failure state managed through conventional MCS compared with the spared single-ventricle (SV), proposed modification

	(*Fontan*) ideal Fontan circulation	(*Fontan*) ideal Fontan circulation (Egbe et al. [12])	(*PVR-Ac*) increased PVR Fontan failure (*Acute*)	(*PVR-Cr*) increased PVR Fontan failure (*Chronic*)	(*PVR-cmcs*) Conventional MCS	(*PVR-switch*) w/ spared SV	(*bPVRtc-switch*) w/ spared SV tachycardia and PA banding	(*bPVRtc-Pswitch*) w/ spared SV pulsatile operation, tachycardia and PA banding
HR (bpm)	70	69 ± 7	70	70	70	70	120	120
EF (%)	44	Echo: 43 ± 4 CMRI: 47 ± 6	42	42	42	43	27	27
Stroke volume index (ml/m^2)	43	Echo: 46 ± 6 CMRI: 45 ± 6	37	40	45	43	25	27
CO (l/min)	4.32	5.76 (4.15–7)	3.69	4.05	4.55	4.32	4.32	4.36
CI (l/min/m^2)	3	3.2 (2.3–3.9)	2.56	2.81	3.16	3	3	3.02
MCS device output (l/min)	n/a	–	n/a	n/a	3	4.32	4.32	4.36
SBP (mmHg)	100	–	90	100	107	–	–	81
DBP (mmHg)	67	n/a	62	65	69	–	–	77
MBP (mmHg)	82	81 ± 5	75	82	88	78	78	79
CVP (mmHg)	14	15 ± 4	16.25	18	15	8.7	9.1	9.25
PAP (mmHg)	10	10 ± 2	12.15	13.5	15	42	37	35

Variations of this Fontan failure state with tachycardia, pulsatile MCS and pulmonary artery (PA) banding is also presented for comparison. The target optimized/healthy Fontan circulation is provided in second column for reference

CI cardiac index, *CMRI* cardiac magnetic resonance imaging, *CO* cardiac output, *CVP* central venous pressure, *DBP* diastolic blood pressure, *EF* ejection fraction, *HR* heart rate, *PAP* pulmonary artery pressure, *SBP* systolic blood pressure, *MBP* mean blood pressure, *MCS* mechanical circulatory support

Additionally, the mean pressure levels of the "weak" SV operating at the pulmonary side was observed to be very similar to that of the native RV. Such desirable hemodynamics is impossible to achieve via the conventional MCS strategies of the Fontan failure. Moreover, subject to the significantly lower afterloads of the right-side, the failing SV at the pulmonary position will start to function at a more favorable operating point, even though it is insufficient to address the higher systemic circulation load demands.

To test the off-design operation of the proposed MCS configuration a mild lower body exercise condition is simulated by our LPM. For this circulation state, Case *VD-switch* provided the required increase in CO and PA pressure by 28% and 35%, respectively while the MCS device output and aortic pressure barely increased (maximum ~ 5%). In contrast to the conventional approach with only the left-sided mechanical support, in spared SV, the sensitivity of PA pressure is much more significant than the sensitivity of aortic pressure to the increased HR metabolic activity. This unique response of the spared-SV configuration is beneficial for stable and balanced left-right hemodynamic coupling.

High PVR Failure Mode

The case *PVR-Cr* represents a high-PVR Fontan failure state, in which the CVP is maintained at 18 mmHg for a long-time, chronically, which is far over the optimal limit (14 mmHg) of an ideal Fontan patient [12, 36]. It is well-established that even a quantum decrease in CVP (2 to 6 mmHg) is effective and will delay the Fontan failure [16, 40, 43, 46]. Correspondingly, in our conventional cavopulmonary support simulations (*PVR-cmcs*) a 3 mmHg drop in CVP achieved which meets the clinical objective and agrees well with the literature. Furthermore, the proposed modification cases with increased PVR Fontan failure (*PVR-switch* and *bPVRtc-Pswitch*) provided further decrease in the CVP (by 9.3 and 8.75 mmHg, respectively), which indicates the effectiveness of this concept.

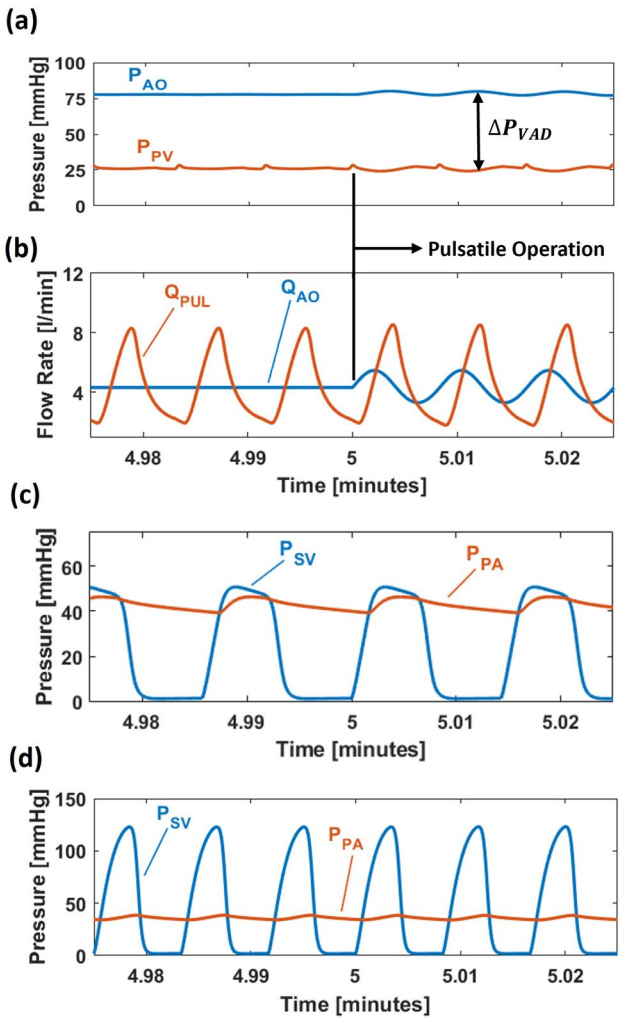

Fig. 7 Fontan Failure Mode 2. Representative hemodynamic waveforms when the high PVR Fontan failure mode is bridged to transplant via the proposed spared single-ventricle (SV) MCS configuration. **a** Aortic (P_{AO}) and pulmonary venous (P_{PV}) chamber pressures, **b** aortic (Q_{AO}) and pulmonary (Q_{PUL}) flow waveforms with the pulsatile MCS device operation, banding and tachycardia (Case *bPVRtc-Pswitch*), **c** single ventricular (P_{SV}) and pulmonary artery (P_{PA}) pressure waveforms without banding and tachycardia (Case *PVR-switch*), and **d** single ventricle (P_{SV}) and pulmonary artery (P_{PA}) pressure waveforms with banding and tachycardia (Case *bPVRtc-switch*). Rotational speed modulation (±400 rpm) to produce pulsatility starts at time = 5 min

Hemodynamic Comparison of Failure Modes

Although the existing concept of creating a biventricular physiology by separating the systemic and pulmonary venous return resembles our proposed modification, the major difference of our concept is that a biventricular support is reconstructed by using one left-sided MCS device [34]. By this way, the complexity pertaining to the use of two separate devices is avoided which is another advantage of this support strategy.

The current concept comprises a ventriculotomy for ventricle-to-PA conduit interposition, which is of concern regarding whether the ventriculotomy-applied ventricle could maintain the pulmonary circulation especially in patients with mildly reduced EF and high PVR. On the contrary, this mildly-failed SV was already supporting the entire circulation before transitioning and would be adequate for the right side. This conclusion was also supported by the findings of the proposed modification for increased PVR model (*PVR-switch*) where SV redundantly supported the pulmonary circulation. Moreover, it led to a considerable increase in the PA pressure reaching to 42 mmHg since the pumping capacity of the even mildly failed SV was considerably higher than a typical RV subject to the Frank–Starling mechanism. This is expected as the rise in PA pressure is likely due to the inability of the downstream pulmonary vascular bed to accommodate the increased CO acutely. The rise in PA pressure is also observed in patients who received heart transplantation or left-ventricular, or bi-ventricular assist device support [15, 16]. For the transplanted failed Fontan patients, this condition generally improves over time through pulmonary vasodilator treatment [3, 4], which is not simulated here. Additionally, if the pulmonary vascular bed preserves its compliance, the rise in PA pressure would be moderately high. Still in failing Fontan patients, due to the pulmonary vasculature remodeling leading to increased trans-pulmonary gradients early after heart transplantation, aggressive use of pulmonary vasodilator therapy is highly recommended [1, 30, 32]. Accordingly, a more effective way of decreasing the PA pressure is attempted here through the *bPVRtc-switch* case employing a banded or an undersized RV-to-PA conduit. This increased resistance led to a one third decrease in PA pressure from 42 to 37 mmHg.

In contrast, for the *VD-switch* case, when a severely failed SV is used in the pulmonary position, excessive pulmonary pressures was not observed due to the lower pumping capacity. This case also provided a significant pulmonary flow pulsatility compared to the high-PVR failure support with the proposed modification (Figs. 5c and 6d). In summary, a failed SV utilized in the pulmonary circulation, which is common for the target clinical problem, will yield healthy hemodynamics at the right-side compared to a mildly reduced SV function in the high PVR case. Accordingly, results revealed that the hemodynamic benefit is more pronounced in patients with low EF, enabling clinicians to utilize even a severely failing ventricle in the systemic circulation on the pulmonary side.

Surgical Risks and Limitations

The surgical reconstruction of the pulmonary venous chamber is the crux of the proposed modification. Due to the low capacity of the pulmonary venous chamber, ~ 25 ml, an

obstruction to the pulmonary venous chamber would lead to critical device malfunction. Despite its complexity, the surgical approach is similar to the already existing Senning procedure [52], which supports the clinical viability of proposed modification. In addition, the literature comprises challenging MCS applications in which the inflow cannula drains directly from the left atrium [6]. For example, in case of an inadequate inflow from the apical SV, De Rita et al. [6] switched the inflow cannula to the CA. Even so, the suctioning effect of a continuous flow MCS device would reflect to the pulmonary venous bed and can inevitably lead to collapse. Still the clinically recorded limit of negative pressure in vacuum-assisted venous return is between − 20 and − 40 mmHg [17], we observed the maximum pressure drop in the pulmonary venous chamber as almost − 1 mmHg. Therefore, it is predicted that the collapse risk is minimal during the clinical application of proposed modification and an average systemic pressure around 90 mmHg to 95 mmHg can easily be achieved without pulmonary venous suctioning effect. Furthermore, a pulsatile extra-corporeal MCS device may be considered due to its effective decompression during pump diastole that is only 60% of each pump cycle [25]. By this way, the uninterrupted suctioning effect of a continuous flow device could be avoided. In addition, the average 40% of blood left in the relatively small pulmonary venous chamber can further prevent its collapse. Finally, highly depending on how atrial septation was made, the current concept would not be suitable for patients with stage III-palliated hypoplastic left heart syndrome due to their innately small left atrial chamber.

Another constraint of the current concept may be associated with ineffective left atrial unloading which will limit the anticipated levels of systemic circulatory support. As a remedy, creating a systemic venous compartment within the Fontan tube graft through taking-down the Fontan graft-right atrial anastomosis, and switching the inflow cannula to the Fontan graft, creating a pulmonary venous atrium through removing the intra-atrial patch, connecting the outflow cannula to the PA or the conduit, and re-opening the aortic valve can be applied. By this way, biventricular circulation can be maintained but with an assisted pulmonary circulation.

The surgical complexity necessitates a back-up plan for the intraoperative failure of the proposed modification. In case of SV failure, rather than using another RVAD replacing the SV, which evolves the system to a BiVAD circulation, the modification will be reversed to a Fontan circulation with TCPC and an LVAD. Another foreseen concern of the current modification is the complexity of the surgical procedure with potentially long cardiopulmonary by-pass times in a patient with an already impaired ventricular function.

While the "double-Hill" ventricle model is validated through literature [37, 66] and it complies with the Frank–Starling mechanism, a better data-driven ventricle function yielding more realistic pressure–volume loops could be developed from the clinical data. As another technical limitation, in our ViVitro piston-pump driven pulse-duplicator, the stroke volume is the only controlling mechanism of the ventricle. This results a system without autoregulation and adaptivity unless the piston pump duty-cycles are controlled via external flow/pressure sensors. Still, the present level of experimental sophistication is adequate since the in vitro experimental results are utilized for the validation of LPM model, and more complex circulation scenarios are investigated only through the computational model. Incorporation of Frank–Starling response in mock-up cardiovascular circuits is an ongoing research challenge [51, 56]. Finally, a constant average friction factor ($f = 0.035$) was used in our computational pump module for simplicity, even though it changes with flow rate. Usage of the exact friction factor for each corresponding flow rate will lead to even better agreement of *in silico* pump characteristic curves with the experimental and literature data (Fig. 2).

Conclusion

Achieving an optimal bridge-to-transplantation management for the failing Fontan circulation through the available MCS devices is an ongoing effort. A consensus on the ideal MCS device implantation strategy has not yet defined due to the limited data and clinical experience as well as large patient-to-patient variation. Even though the detailed *in vitro* and *in silico* simulations of the proposed concept demonstrated encouraging results in terms of biventricular pressure and flow levels, it is essential to test this proof-of-concept idea in an animal model. This step is essential as the use of failed-SV as a pulsatile pump is planned for the long-term support as a bridge to transplantation. In conclusion, specially targeting the low resource settings with limited access to MCS devices and heart transplantation, sparing the native ventricle as a right-heart support will provide a novel perspective for MCS device implantation in failed Fontan patients.

Appendix 1

See Tables 5, 6, and 7.

Table 5 Compliance data used in case *Fontan*

	Chamber	Parameter			
		C (l/mmHg)	$C_{systolic}$ (l/mmHg)	$C_{diastolic}$ (l/mmHg)	Sample mean pressure of key components (mmHg)
1	Single ventricle (SV)		1.10E−03	6.50E−02	39.6
2	Aortic arch (AoA)	3.21E−05			70.6
3	Upper body (UB)	4.60E−03			
4	Lower body (LB)	5.30E−06			
5	Superior vena cava (SVC)	5.40E−03			13
6	Inferior vena cava (IVC)	3.22E−04			14
7	Pulmonary artery (PA) (RPA + LPA)	2.14E−04			10.7
8	Lungs (LUNG)	3.30E−03			
9	Common atrium (CA)		6.30E−03	4.80E−03	6.2

Table 6 Compliance data used in case *VD-Cr* and *VD-cmcs*

	Chamber	Parameter			
		C (l/mmHg)	$C_{systolic}$ (l/mmHg)	$C_{diastolic}$ (l/mmHg)	Sample mean pressure of key components (mmHg)
1	Single ventricle (SV)		1.70E−03	3.80E−02	32
2	Aortic arch (AoA)	4.80E−05			65.4
3	Upper body (UB)	4.30E−03			
4	Lower body (LB)	5.00E−06			
5	Superior vena cava (SVC)	5.00E−03			10
6	Inferior vena cava (IVC)	3.00E−03			10.8
7	Pulmonary artery (PA) (RPA + LPA)	2.00E−04			
8	Lungs (LUNG)	3.00E−03			
9	Common atrium (CA)		5.90E−03	4.50E−03	6

Table 7 Compliance data used in case *VD-switch*

	Chamber	Parameter			
		C (l/mmHg)	$C_{systolic}$ (l/mmHg)	$C_{diastolic}$ (l/mmHg)	Sample mean pressure of key components (mmHg)
1	Single ventricle (SV)		5.60E−03	3.50E−02	18.5
2	Aortic arch (AoA)	4.80E−05			101
3	Upper body (UB)	4.30E−03			
4	Lower body (LB)	5.00E−06			
5	Superior vena cava (SVC)	5.00E−03			11.5
6	Inferior vena cava (IVC)	3.00E−03			12
7	Pulmonary artery (PA) (RPA + LPA)	2.00E−04			17.5
8	Lungs (LUNG)	3.00E−03			
9	**Right Atrium (RA)**		**4.70E−03**	**3.20E−03**	9.5
10	**Posterior pulmonary venous (PV)**		**1.82E−04**	**1.38E−04**	− 1.5

Bold represents the newly created chambers in this case

Appendix 2

See Tables 8, 9, and 10.

Table 8 Resistance data used in case *Fontan*

	Vessel	Connection			Valved flow		Sample mean flow rate of key components (l/min)
		Chamber 1	Chamber 2	$R_{1\leftrightarrow 2}$ [mmHg/(l/min)]	$R_{1\rightarrow 2}$ [mmHg/(l/min)]	$R_{2\rightarrow 1}$ [mmHg/(l/min)]	
1	Aortic valve (R_{Ao})	1	2		0.25	Inf	4.92
2	Upper body 1 (R_{ub1})	2	3	$R_{ub1}+R_{ub2}=29.6$			1.95
4	Upper body 2 (R_{ub2})	3	5				
5	Lower body 1 (R_{lb1})	2	4	$R_{lb1}+R_{lb2}=19$			2.97
6	Lower body 2 (R_{lb2})	4	6				
7	TCPC 1	5	7	1.0			1.95
8	TCPC 2	6	7	1.1			2.97
9	Pulmonary artery (R_{pa})	7	8	$R_{rpa}+R_{lpa}=0.85$			4.92
10	Pulmonary veins (R_{pv})	8	9	0.55			4.92
11	Atrioventricular valve	9	10		0.125	Inf	4.92

Table 9 Resistance data used in case *VD-Cr* and *VD-cmcs*

	Vessel	Connection			Valved flow		Sample mean flow rate of key components (l/min)
		Chamber 1	Chamber 2	$R_{1\leftrightarrow 2}$ [mmHg/(l/min)]	$R_{1\rightarrow 2}$ [mmHg/(l/min)]	$R_{2\rightarrow 1}$ [mmHg/(l/min)]	
1	Aortic valve (R_{Ao})	1	2		0.25	Inf	2.47
2	Upper body 1 (R_{ub1})	2	3	$R_{ub1}+R_{ub2}=31.2$			0.98
4	Upper body 2 (R_{ub2})	3	5				
5	Lower body 1 (R_{lb1})	2	4	$R_{lb1}+R_{lb2}=20$			1.49
6	Lower body 2 (R_{lb2})	4	6				
7	TCPC 1	5	7	1.0			0.98
8	TCPC 2	6	7	1.2			1.49
9	Pulmonary artery (R_{pa})	7	8	$R_{rpa}+R_{lpa}=0.9$			2.47
10	Pulmonary veins (R_{pv})	8	9	0.55			2.47
11	Atrioventricular valve	9	10		0.125	Inf	2.47

Table 10 Resistance data used in case *VD-switch*

	Vessel	Connection			Valved flow		Sample mean flow rate of key components (l/min)	
		Chamber 1	Chamber 2	$R_{1\leftrightarrow 2}$ [mmHg/(l/min)]	$R_{1\rightarrow 2}$ [mmHg/(l/min)]	$R_{2\rightarrow 1}$ [mmHg/(l/min)]		
1	**MCSD-Aorta graft**	**10**	**2**	**n/a (Pump flow)**			4.95	**Systemic circulation governed by the MCSD**
2	Upper body 1 (R_{ub1})	2	3	$R_{ub1}+R_{ub2}=31.2$			1.96	
4	Upper body 2 (R_{ub2})	3	5					
5	Lower body 1 (R_{lb1})	2	4	$R_{lb1}+R_{lb2}=20$			2.99	
6	Lower body 2 (R_{lb2})	4	6					
7	**Systemic veins (R_{sv})**	**5**	**9**	**0.1**	**6**	**9**	4.95	
8	Atrioventricular valve	9	1		0.125	Inf	4.95	**Pulmonary circulation governed by the SV**
8	**SV-PA conduit**	**1**	**7**	**0.25**			4.95	
9	Pulmonary artery (R_{pa})	7	8	$R_{rpa}+R_{lpa}=0.9$			4.95	
10	Pulmonary veins (R_{pv})	8	9	0.55			4.95	

Bold represents the newly created connections between the chambers in this case

Acknowledgements We would like to express our gratitude to Medtronic for providing a loaner HeartWare MCS pump during the *in vitro* experiments.

Author Contributions ES, ONT, YA, MO, KP hypothesized and introduced the proposed concept. CY, BA, KP designed and conducted computational and experimental work. All authors wrote and edited the manuscript text.

Funding Funding was provided by Research Grants from the European Research Council (ERC) Proof of Concept 966765 *BloodTurbine,* TUBITAK *118M369 and* TUBITAK *118S108* (*PI: Kerem Pekkan*).

Data Availability There are no restrictions on the availability of materials or information. The compliance and resistance parameters with the datasets generated and/or analyzed during the current study are available via https://doi.org/10.5281/zenodo.6300829. For any questions, please contact corresponding authors.

Declarations

Conflict of interest KP and CY hold patents on Fontan assist devices but not directly related to the proposed configuration. Authors have no other conflict of interest.

References

1. Bernstein, D., D. Naftel, C. Chin, L. J. Addonizio, P. Gamberg, E. D. Blume, D. Hsu, C. E. Canter, J. K. Kirklin, W. R. Morrow, Society for Pediatric Heart Transplantation. Outcome of listing for cardiac transplantation for failed Fontan: a multi-institutional study. *Circulation*. 114:273–280, 2006.
2. Birati, E. Y., and J. E. Rame. Left ventricular assist device management and complications. *Crit. Care Clin.* 30:607–627, 2014.
3. Cardoso, B., A. Kelecsenyi, J. Smith, K. Jansen, F. De Rita, M. S. Nassar, and L. Coats. Improving outcomes for transplantation in failing Fontan—what is the next target? *JTCVS Open*. 8:565–573, 2021.
4. Cilliers, A., and M. Gewillig. Fontan procedure for univentricular hearts: have changes in design improved outcome? *Cardiovasc. J. S. Afr.* 13:111–116, 2002.
5. De Rita, F., D. Crossland, M. Griselli, and A. Hasan. Management of the failing Fontan. *Semin. Thorac. Cardiovasc. Surg. Pediatr. Card. Surg. Annu.* 18:2–6, 2015.
6. De Rita, F., A. Hasan, S. Haynes, D. Crossland, R. Kirk, L. Ferguson, E. Peng, and M. Griselli. Mechanical cardiac support in children with congenital heart disease with intention to bridge to heart transplantation. *Eur. J. Cardiothorac. Surg.* 46:656–662, 2014.
7. Di Molfetta, A., A. Amodeo, L. Fresiello, S. Filippelli, M. Pilati, R. Iacobelli, R. Adorisio, D. Colella, and G. Ferrari. The use of a numerical model to simulate the cavo-pulmonary assistance in Fontan circulation: a preliminary verification. *J. Artif. Organs*. 19:105–113, 2016.
8. Di Molfetta, A., A. Amodeo, M. G. Gagliardi, M. G. Trivella, L. Fresiello, S. Filippelli, A. Toscano, and G. Ferrari. Hemodynamic effects of ventricular assist device implantation on Norwood, Glenn, and Fontan circulation: a simulation study. *Artif. Organs*. 40:34–42, 2016.
9. Doyle, M. G., M. Chugunova, S. L. Roche, and J. P. Keener. Lumped parameter models for two-ventricle and healthy and

failing extracardiac Fontan circulations. *Math. Med. Biol.* 38:442–466, 2021.
10. Dur, O., M. Lara, D. Arnold, S. Vandenberghe, B. B. Keller, C. DeGroff, and K. Pekkan. Pulsatile in vitro simulation of the pediatric univentricular circulation for evaluation of cardiopulmonary assist scenarios. *Artif. Organs*. 33:967–976, 2009.
11. Durham III, L. A., J. A. Dearani, H. M. Burkhart, L. D. Joyce, F. Cetta Jr., A. K. Cabalka, S. D. Phillips, K. Sundareswaran, D. Farrar, and S. J. Park. Application of computer modeling in systemic VAD support of failing Fontan physiology. *World J. Pediatr. Congenit. Heart Surg.* 2:243–248, 2011.
12. Egbe, A. C., H. M. Connolly, W. R. Miranda, N. M. Ammash, D. J. Hagler, G. R. Veldtman, and B. A. Borlaug. Hemodynamics of Fontan failure: the role of pulmonary vascular disease. *Circ. Heart Fail.*10(12):e004515, 2017.
13. Farahmand, M., M. N. Kavarana, and E. O. Kung. Risks and benefits of using a commercially available ventricular assist device for failing Fontan cavopulmonary support: a modeling investigation. *IEEE Trans. Biomed. Eng.* 67:213–219, 2020.
14. Fontan, F., and E. Baudet. Surgical repair of tricuspid atresia. *Thorax*. 26:240–248, 1971.
15. Fukamachi, K., A. Shiose, A. L. Massiello, D. J. Horvath, L. A. Golding, S. Lee, and R. C. Starling. Implantable continuous-flow right ventricular assist device: lessons learned in the development of a Cleveland Clinic device. *Ann. Thorac. Surg.* 93:1746–1752, 2012.
16. Gandolfo, F., G. Brancaccio, S. Donatiello, S. Filippelli, G. Perri, E. Iannace, D. D'Amario, G. Testa, G. D'Avenio, M. Grigioni, and A. Amodeo. Mechanically assisted total cavopulmonary connection with an axial flow pump: computational and in vivo study. *Artif. Organs*. 40:43–49, 2016.
17. Gao, S., Y. Li, X. Diao, S. Yan, G. Liu, M. Liu, Q. Zhang, W. Zhao, and B. Ji. Vacuum-assisted venous drainage in adult cardiac surgery: a propensity-matched study. *Interact. Cardiovasc. Thorac. Surg.* 30:236–242, 2020.
18. Giridharan, G. A., S. C. Koenig, J. Kennington, M. A. Sobieski, J. Chen, S. H. Frankel, and M. D. Rodefeld. Performance evaluation of a pediatric viscous impeller pump for Fontan cavopulmonary assist. *J. Thorac. Cardiovasc. Surg.* 145:249–257, 2013.
19. Good, B. C., S. V. Ponnaluri, W. J. Weiss, and K. B. Manning. Computational modeling of the Penn State Fontan circulation assist device. *ASAIO J.* 68:1513–1522, 2022.
20. Granegger, M., M. Schweiger, M. Schmid Daners, M. Meboldt, and M. Hübler. Cavopulmonary mechanical circulatory support in Fontan patients and the need for physiologic control: a computational study with a closed-loop exercise model. *Int. J. Artif. Organs*. 41:261–268, 2018.
21. Hasegawa, M., Y. Tominaga, T. Watanabe, T. Ueno, M. Taira, and S. Miyagawa. Successful bridge to transplantation with long-term support using Berlin heart EXCOR in a child with failing Fontan. *Gen. Thorac. Cardiovasc. Surg.* 70:750–753, 2022.
22. Heidenreich, P. A., B. Bozkurt, D. Aguilar, L. A. Allen, J. J. Byun, M. M. Colvin, A. Deswal, M. H. Drazner, S. M. Dunlay, L. R. Evers, J. C. Fang, S. E. Fedson, G. C. Fonarow, S. S. Hayek, A. F. Hernandez, P. Khazanie, M. M. Kittleson, C. S. Lee, M. S. Link, C. A. Milano, L. C. Nnacheta, A. T. Sandhu, L. W. Stevenson, O. Vardeny, A. R. Vest, and C. W. Yancy. 2022 AHA/ACC/HFSA guideline for the management of heart failure: executive summary: a Report of the American College of Cardiology/American Heart Association Joint Committee on Clinical Practice Guidelines. *Circulation*. 145:e876–e894, 2022.
23. Hernandez, J., S. G. Chopski, S. Lee, W. B. Moskowitz, and A. L. Throckmorton. Externally applied compression therapy for Fontan patients. *Transl. Pediatr.* 7:14–22, 2018.
24. Hoffman, J. I., and S. Kaplan. The incidence of congenital heart disease. *J. Am. Coll. Cardiol.* 39:1890–1900, 2002.
25. Horne, D., J. Conway, I. M. Rebeyka, and H. Buchholz. Mechanical circulatory support in univentricular hearts: current management. *Semin. Thorac. Cardiovasc. Surg. Pediatr. Card. Surg. Annu.* 18:17–24, 2015.
26. Jaquiss, R. D., and H. Aziz. Is four stage management the future of univentricular hearts? Destination therapy in the young. *Semin. Thorac. Cardiovasc. Surg. Pediatr. Card. Surg. Annu.* 19:50–54, 2016.
27. Karimov, J. H., K. Fukamachi, and R. C. Starling. Mechanical Support for Heart Failure: Current Solutions and New Technologies. Berlin: Springer, 2020.
28. Koçyıldırım, E., O. Dur, O. Soran, E. Tüzün, M. W. Miller, G. J. Housler, P. D. Wearden, T. W. Fossum, V. O. Morell, and K. Pekkan. Pulsatile venous waveform quality in Fontan circulation—clinical implications, venous assists options and the future. *Anadolu Kardiyol. Derg*. 12:420–426, 2012.
29. Kung, E., G. Pennati, F. Migliavacca, T. Y. Hsia, R. Figliola, A. Marsden, A. Giardini, and M. Investigators. A simulation protocol for exercise physiology in Fontan patients using a closed loop lumped-parameter model. *J. Biomech. Eng.* 136:0810071–08100714, 2014.
30. Lammers, A. E., and T. Humpl. Use of pulmonary vasodilators in Fontan patients: a useful strategy to improve functional status and delay transplantation? *Pulm. Circ.* 8:2045894018798616, 2018.
31. Lin, W. C. P., M. G. Doyle, S. L. Roche, O. Honjo, T. L. Forbes, and C. H. Amon. Computational fluid dynamic simulations of a cavopulmonary assist device for failing Fontan circulation. *J. Thorac. Cardiovasc. Surg.* 158:1424-1433.e1425, 2019.
32. McCormick, A. D., and K. R. Schumacher. Transplantation of the failing Fontan. *Transl. Pediatr.* 8:290–301, 2019.
33. Moazami, N., K. Fukamachi, M. Kobayashi, N. G. Smedira, K. J. Hoercher, A. Massiello, S. Lee, D. J. Horvath, and R. C. Starling. Axial and centrifugal continuous-flow rotary pumps: a translation from pump mechanics to clinical practice. *J. Heart Lung Transplant.* 32:1–11, 2013.
34. Nathan, M., C. Baird, F. Fynn-Thompson, C. Almond, R. Thiagarajan, P. Laussen, E. Blume, and F. Pigula. Successful implantation of a Berlin Heart biventricular assist device in a failing single ventricle. *J. Thorac. Cardiovasc. Surg.* 131:1407–1408, 2006.
35. Noor, M. R., C. H. Ho, K. H. Parker, A. R. Simon, N. R. Banner, and C. T. Bowles. Investigation of the characteristics of HeartWare HVAD and Thoratec Heart Mate II under steady and pulsatile flow conditions. *Artif. Organs*. 40:549–560, 2016.
36. Ohuchi, H. Where is the "Optimal" Fontan hemodynamics? *Korean Circ. J.* 47:842–857, 2017.
37. Peer, S. M., C. Yildirim, M. Desai, K. Ramakrishnan, P. Sinha, R. Jonas, C. Yerebakan, and K. Pekkan. Mechanical support of pulmonary blood flow as a strategy to support the Norwood circulation-lumped parameter model study. *Eur. J. Cardiothorac. Surg.* 62(1):ezac262, 2022.
38. Pekkan, K., I. B. Aka, E. Tutsak, E. Ermek, H. Balim, I. Lazoglu, and R. Turkoz. In vitro validation of a self-driving aortic-turbine venous-assist device for Fontan patients. *J. Thorac. Cardiovasc. Surg.* 156:292-301.e297, 2018.
39. Pekkan, K., D. Frakes, D. De Zelicourt, C. W. Lucas, W. J. Parks, and A. P. Yoganathan. Coupling pediatric ventricle assist devices to the Fontan circulation: simulations with a lumped-parameter model. *ASAIO J.* 51:618–628, 2005.
40. Pekkan, K., H. D. Kitajima, D. de Zelicourt, J. M. Forbess, W. J. Parks, M. A. Fogel, S. Sharma, K. R. Kanter, D. Frakes, and A. P. Yoganathan. Total cavopulmonary connection flow with functional left pulmonary artery stenosis: angioplasty and fenestration in vitro. *Circulation*. 112:3264–3271, 2005.

41. Prather, R., A. Das, M. Farias, E. Divo, A. Kassab, and W. DeCampli. Parametric investigation of an injection-jet self-powered Fontan circulation. *Sci. Rep.* 12:2161, 2022.
42. Presson Jr., R. G., W. A. Baumgartner Jr., A. J. Peterson, R. W. Glenny, and W. W. Wagner Jr. Pulmonary capillaries are recruited during pulsatile flow. *J. Appl. Physiol. (1985)* 92:1183–1190, 2002.
43. Rehan, R., I. Kotchetkova, R. Cordina, and D. Celermajer. Adult congenital heart disease survivors at age 50 years: medical and psychosocial status. *Heart Lung Circ.* 30:261–266, 2021.
44. Reller, M. D., M. J. Strickland, T. Riehle-Colarusso, W. T. Mahle, and A. Correa. Prevalence of congenital heart defects in metropolitan Atlanta, 1998–2005. *J. Pediatr.* 153:807–813, 2008.
45. Rich, J. D., and D. Burkhoff. HVAD flow waveform morphologies: theoretical foundation and implications for clinical practice. *ASAIO J.* 63:526–535, 2017.
46. Rodefeld, M. D., J. H. Boyd, C. D. Myers, B. J. LaLone, A. J. Bezruczko, A. W. Potter, and J. W. Brown. Cavopulmonary assist: circulatory support for the univentricular Fontan circulation. *Ann. Thorac. Surg.* 76:1911–1916; discussion 1916, 2003.
47. Rychik, J. The relentless effects of the Fontan paradox. *Semin. Thorac. Cardiovasc. Surg. Pediatr. Card. Surg. Annu.* 19:37–43, 2016.
48. Rychik, J., A. M. Atz, D. S. Celermajer, B. J. Deal, M. A. Gatzoulis, M. H. Gewillig, T. Y. Hsia, D. T. Hsu, A. H. Kovacs, B. W. McCrindle, J. W. Newburger, N. A. Pike, M. Rodefeld, D. N. Rosenthal, K. R. Schumacher, B. S. Marino, K. Stout, G. Veldtman, A. K. Younoszai, Y. d'Udekem, American Heart Association Council on Cardiovascular Disease in the Young and Council Cardiovascular and Stroke Nursing. Evaluation and management of the child and adult with Fontan circulation: a scientific statement from the American Heart Association. *Circulation*. 140(6):e234–e284, 2019.
49. Schilling, C., K. Dalziel, R. Nunn, K. Du Plessis, W. Y. Shi, D. Celermajer, D. Winlaw, R. G. Weintraub, L. E. Grigg, D. J. Radford, A. Bullock, T. L. Gentles, G. R. Wheaton, T. Hornung, R. N. Justo, and Y. d'Udekem. The Fontan epidemic: population projections from the Australia and New Zealand Fontan Registry. *Int. J. Cardiol.* 219:14–19, 2016.
50. Shimizu, S., D. Une, T. Kawada, Y. Hayama, A. Kamiya, T. Shishido, and M. Sugimachi. Lumped parameter model for hemodynamic simulation of congenital heart diseases. *J. Physiol. Sci.* 68:103–111, 2018.
51. Siewnicka, A., K. Janiszowski, and M. Gawlikowski. A physical model of the human circulatory system for the modeling, control and diagnostic of cardiac support processes. In: *Mechatronics 2013: Recent Technological and Scientific Advances.* Berlin: Springer, 2014, pp. 825–832.
52. Stark, J. Modified Senning operation for cavopulmonary connection with autologous tissue. *J. Thorac. Cardiovasc. Surg.* 109:1264, 1995.
53. Stergiopulos, N., J. J. Meister, and N. Westerhof. Determinants of stroke volume and systolic and diastolic aortic pressure. *Am. J. Physiol.* 270:H2050–H2059, 1996.
54. Suga, H., K. Sagawa, and A. A. Shoukas. Load independence of the instantaneous pressure–volume ratio of the canine left ventricle and effects of epinephrine and heart rate on the ratio. *Circ. Res.* 32:314–322, 1973.
55. Telyshev, D., M. Denisov, A. Markov, L. Fresiello, T. Verbelen, and S. Selishchev. Energetics of blood flow in Fontan circulation under VAD support. *Artif. Organs*. 44:50–57, 2020.
56. Telyshev, D. V., A. A. Pugovkin, I. A. Ephimov, A. Markov, S. Leonhardt, M. Walter, J. H. Karimov, and S. V. Selishchev. Correlation between myocardial function and electric current pulsatility of the Sputnik left ventricular assist device: in vitro study. *Appl. Sci.* 11:3359, 2021.
57. Tree, M., P. M. Trusty, T. C. Slesnick, A. Yoganathan, S. Deshpande, and K. Maher. In vitro examination of the HeartWare CircuLite ventricular assist device in the Fontan connection. *ASAIO J.* 63:482–489, 2017.
58. Trusty, P. M., M. Tree, K. Maher, T. C. Slesnick, K. R. Kanter, A. P. Yoganathan, and S. R. Deshpande. An in vitro analysis of the PediMag and CentriMag for right-sided failing Fontan support. *J. Thorac. Cardiovasc. Surg.* 158:1413–1421, 2019.
59. Valdovinos, J., E. Shkolyar, G. P. Carman, and D. S. Levi. In vitro evaluation of an external compression device for Fontan mechanical assistance. *Artif. Organs*. 38:199–207, 2014.
60. Wang, D., G. Gao, M. Plunkett, G. Zhao, S. Topaz, C. Ballard-Croft, and J. B. Zwischenberger. A paired membrane umbrella double-lumen cannula ensures consistent cavopulmonary assistance in a Fontan sheep model. *J. Thorac. Cardiovasc. Surg.* 148:1041–1047; discussion 1047, 2014.
61. Warnes, C. A., R. Liberthson, G. K. Danielson, A. Dore, L. Harris, J. I. Hoffman, J. Somerville, R. G. Williams, and G. D. Webb. Task Force 1: the changing profile of congenital heart disease in adult life. *J. Am. Coll. Cardiol.* 37:1170–1175, 2001.
62. Weinstein, S., R. Bello, C. Pizarro, F. Fynn-Thompson, J. Kirklin, K. Guleserian, R. Woods, C. Tjossem, R. Kroslowitz, P. Friedmann, and R. Jaquiss. The use of the Berlin Heart EXCOR in patients with functional single ventricle. *J. Thorac. Cardiovasc. Surg.* 147:697–705, 2014.
63. Woods, R. K., N. S. Ghanayem, M. E. Mitchell, S. Kindel, and R. A. Niebler. Mechanical circulatory support of the Fontan patient. *Semin. Thorac. Cardiovasc. Surg. Pediatr. Card. Surg. Annu.* 20:20–27, 2017.
64. Yamada, A., Y. Shiraishi, H. Miura, H. M. Hashem, Y. Tsuboko, M. Yamagishi, and T. Yambe. Development of a thermodynamic control system for the Fontan circulation pulsation device using shape memory alloy fibers. *J. Artif. Organs*. 18:199–205, 2015.
65. Yigit, B., E. Tutsak, C. Yildirim, D. Hutchon, and K. Pekkan. Transitional fetal hemodynamics and gas exchange in premature postpartum adaptation: immediate vs. delayed cord clamping. *Matern. Health Neonatol. Perinatol.* 5:5, 2019.
66. Yigit, M. B., W. J. Kowalski, D. J. Hutchon, and K. Pekkan. Transition from fetal to neonatal circulation: modeling the effect of umbilical cord clamping. *J. Biomech.* 48:1662–1670, 2015.

Authors and Affiliations

Emrah Şişli[1] · Canberk Yıldırım[2] · İbrahim Başar Aka[3] · Osman Nuri Tuncer[4] · Yüksel Atay[4] · Mustafa Özbaran[5] · Kerem Pekkan[6]

✉ Emrah Şişli
emrah.sisli@ogu.edu.tr

✉ Kerem Pekkan
kpekkan@ku.edu.tr

[1] Pediatric Cardiovascular Surgery, Department of Cardiovascular Surgery, Osmangazi University Faculty of Medicine, Büyükdere District, Campus of Meşelik, Tepebaşı, 26480 Eskisehir, Turkey

[2] Department of Biomedical Sciences and Engineering, Koç University, Istanbul, Turkey

[3] Department of Mechatronics Engineering, İstanbul Bilgi University, Istanbul, Turkey

[4] Pediatric Cardiovascular Surgery, Department of Cardiovascular Surgery, Ege University Faculty of Medicine, Izmir, Turkey

[5] Heart Transplantation, Department of Cardiovascular Surgery, Ege University Faculty of Medicine, Izmir, Turkey

[6] Department of Mechanical Engineering, Koç University, Rumeli Feneri Campus, Sarıyer, Istanbul, Turkey